Short-term retention in metallic PFCs: modelling in view of mass spectrometry and LIBS

Dmitry Matveev, Xi Jiang, Gennady Sergienko, Arkadi Kreter, Sebastijan Brezinsek and Christian Linsmeier

Forschungszentrum Jülich GmbH, EURATOM Association, 52425 Juelich, Germany

E-mail: d.matveev@fz-juelich.de

Received xxxxxx
Accepted for publication xxxxxx
Published xxxxxx

Abstract

Based on the conventional model of hydrogen retention in plasma-facing components, the question of hydrogen outgassing during and after plasma exposure is addressed in relation to mass spectrometry and laser-induced breakdown sprectroscopy (LIBS) measurements. Fundamental differences in retention and release data acquired by LIBS and by mass spectrometry are described analytically and by modelling. Reaction-diffusion simulations are presented that demonstrate possible thermal outgassing effects caused by LIBS. Advantages and limitations of LIBS as a tool for analysis of short term retention are discussed.

Keywords: hydrogen retention, dynamic outgassing, mass spectrometry, LIBS

1. Introduction

Short-term retention in metallic plasma-facing components such as tungsten (W) is associated with mobile interstitial and weakly trapped hydrogen introduced into the material by plasma exposure. The influx of atoms by implantation drives the growth of the interstitial hydrogen (iH) concentration and leads to concentration gradients. During exposure, iH atoms are constantly re-emitted as molecules due to diffusion, recombination and desorption, and this process is referred to as recycling. When the implantation source is removed, iH atoms continue to be re-emitted, leading to a reduction of the iH concentration. This shifts the local dynamic trapping-detrapping balance so that hydrogen from weak trapping sites can be released, which feeds the iH population for much longer times than the classical characteristic time of diffusion. The flux of hydrogen released this way from plasma-exposed surfaces is referred to as dynamic outgassing. The word “dynamic” indicates the implantation-induced nature of release as opposed to thermal degassing of intrinsic hydrogen. We shall call this process passive outgassing to distinguish it from outgassing stimulated by a temperature increase, e.g. in thermal desorption spectroscopy (TDS) or laser heating.

The total amount of hydrogen released passively within minutes, hours or days after exposure is referred to as short-term retention. Long-term retention, in opposite, is attributed to hydrogen that is strongly bound to defects or impurities and therefore remains almost immobile on the time scale of days, months or even years. The sample temperature after exposure and during storage can notably alter the ratio between the short-term and long-term retention.

It is difficult to access the dynamics of short-term retention experimentally since techniques such as e.g. TDS are typically applied hours or days after exposure, thus disclosing only somewhat "longer"-term retention [1]. Using mass spectrometry [2] one can monitor the outgassing fluxes from exposed surfaces and thus determine retention as the difference between known injected and measured released amounts of gas. Though offering reasonable time resolution, this global method cannot resolve local variations of retention between different locations. New interesting perspectives for inferring the local short-term retention dynamics are offered by laser-induced breakdown spectroscopy (LIBS) [3]. LIBS is capable of in-situ, local and time-resolved measurements of hydrogen content.

A LIBS system has been developed and installed on the linear plasma device PSI-2 [4, 5] and first measurements of deuterium (D) content in exposed W samples during and after exposure to D plasma have been performed [6]. This paper is intended to help interpret experimental results. In section 2, we briefly review the conventional mechanisms of retention and outgassing and discuss the relation between data obtained from mass spectrometry and LIBS. Section 3 provides an analysis of D release by dynamic outgassing and LIBS with modelling examples aligned with experiments in PSI-2. Concluding remarks follow in section 4.

2. Mass spectrometry vs LIBS

In the nuclear fusion context, experiments are typically performed using D to distinguish it from the naturally present protium (H). Outgassing is monitored with mass spectrometry so that signals proportional to the partial pressures of D_2 and HD are measured. The total D retention is assessed by TDS.

LIBS uses a short duration focused high power laser beam to ablate a small amount of material. Interaction of the laser with the ablated material creates a local plasma that expands and emits characteristic light spectrum that contains information about atomic species and their quantities in the ablated material. Extremely short (fs – ps) laser pulses, lead to "cold" ablation with no or minimal heating of the sample [8]. For longer pulses (ns), electron diffusion and energy transfer to the lattice lead to sample heating also beyond the ablated region [9]. This can lead to additional outgassing due to thermal effects and may be not fully quantifiable by spectroscopic observations due to delayed release by desorption. Even longer pulse durations (ms) correspond to laser induced desorption (LID) [7]. The PSI-2 LIBS setup [5, 6] uses a Nd:YAG laser at a wavelength of 532 nm, with pulse length of about 8.3 ns and the beam energy of 400 mJ, which leads to a single-pulse ablation of $\sim$100 nm layer of W (laser beam spot $\sim 1\ \mathrm{mm}^2$). Some thermal effects can be expected in this case and will be addressed in section 3. In order to assess the dynamics of short-term retention, a sequence of LIBS measurements at adjacent positions on the sample surface is performed and thus the amount of retained D at different times during or after exposure is obtained. The difference between two subsequent measurements corresponds to D release in the respective time interval.

According to [10] and works referenced therein, D retention in W in laboratory studies can be well described assuming three types of traps: two uniformly distributed intrinsic trap types and one ion-induced and thus fluence dependent trap type localized near the surface. The concentration of ion-induced traps is assumed to saturate at high fluences, which means that for long enough exposure times the total retention will be dominated by diffusion-driven population of intrinsic traps. This fact is supported by high fluence exposures in the linear plasma device PISCES-B [11], where a square-root of time dependence of total retention was

measured up to a maximum D fluence of 2×10^{28} m^{-2}. In the initial phase, however, trap-creation in the near-surface region should result in a steeper fluence dependence.

The recycling coefficient R, calculated as the ratio of the escaping flux (atoms/s) to the incoming non-reflected ion flux (ions/s), is a measure of outgassing during plasma exposure. The value of R is close to unity under steady state plasma conditions and readjusts very fast to changes such as e.g. during edge-localized modes [12]. For all practical exposure times, outgassing during exposure to steady state plasma remains constant, except for the initial phase when the near-surface profile of interstitial D is being established by implantation.

Passive D outgassing after exposure in present day tokamaks is well described by the empirical power law decay of flux with time after exposure: $F(t) \sim t^a$. Values of the exponent $a = -0.7 \pm 0.2$ have been reported, being rather independent from wall materials and exposure conditions [13-17]. In PSI-2 a decay with $a \cong -1$ was measured for a bulk W target [18]. Several attempts of mathematical and computational analysis of post-discharge outgassing have been made to explain the observed power law decay of the outgassing flux [13, 19-24]. In the following we shall stick to power law as a good approximation for post-discharge outgassing and assume it to be an objective consequence of local physical processes.

Figure 1 summarises the views and assumptions discussed above, bridging the retention and outgassing perspectives for short-term and long-term retention. In the upper frame a sketch of time evolution of the outgassing flux from the beginning of plasma exposure and beyond the end of plasma exposure is shown. Outgassing flux approaches the incoming ion flux and remains constant until the end of exposure. After exposure, outgassing follows the power law decay $F(t) = F_0 \cdot (t/t_o)^a$, where t_0 is the plasma-off time and F_0 corresponds to the recycling flux during exposure. The outgassing flux tends to zero at very large t. The integral of the outgassing flux gives the amount of D released up to a given point of time:

$$R_{\mathrm{rel}}(t) = F_0 \int_{t_0}^{t} \left(\frac{t'}{t_0}\right)^a dt' = \frac{F_0 t_0}{a+1}\left(\left(\frac{t}{t_0}\right)^{a+1} - 1\right). \quad (1)$$

The middle frame in figure 1 shows in parallel the evolution of total retention. During plasma exposure retention grows with (at least) a square-root of time dependence, reaching the value R_{tot} corresponding to total retention at the end of exposure. After exposure the amount of retainted D gradually decreases due to outgassing and in long term approaches a constant value R_∞, the long-term retention. According to equation 1, retention as a function of time after exposure can be written as

$$R(t) = R_{\mathrm{tot}} - R_{\mathrm{rel}}(t) = R_{\mathrm{tot}} - \frac{F_0 t_0}{a+1}\left(\left(\frac{t}{t_0}\right)^{a+1} - 1\right), \quad (2)$$

which means that it also follows a power law decay (as long as the outgassing flux follows the power law decay), however with an exponent $a + 1$. Physically, power law of outgassing cannot last forever and has to transition to exponential decay at some point.

During a LIBS pulse the material is ablated leaving a crater of a finite depth. Thermal release due to heat propagation is also limited (section 3). This means that the information depth of LIBS is restricted to the thickness of ablation plus potential heat affected zone. This is illustrated in the lower frame in figure 1 where evolution of retention is shown for a surface layer corresponding to the information depth of LIBS. In this case retention grows in the initial phase, but saturates when diffusion front passes deeper than the respective layer thickness or, in case of trap creation, when ion-induced traps in the layer saturate. After exposure retention decreases due to outgassing, however, since the surface layer analyzed by LIBS constitutes only a fraction of total retention, the decay of retention in this zone should not necessarily follow that of total retention. Also the resulting long-term retention in the layer will be expectedly less than total retention, unless the measurement is performed after a short exposure when D atoms had not time to permeate deeper.

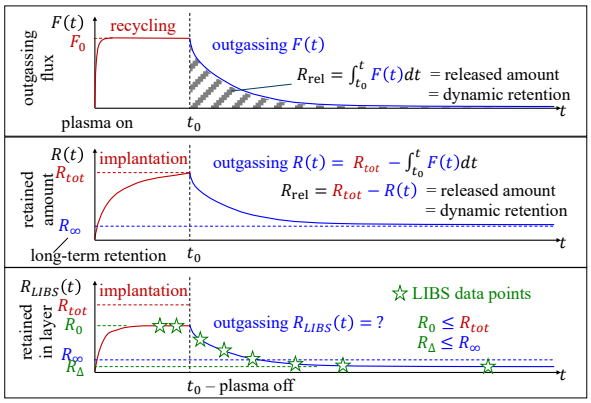

Figure 1. Illustration of evolution of the outgassing flux (upper frame), total retention (middle frame) and retention in a surface layer corresponding to the information depth of LIBS during and after plasma exposure.

3. D release by dynamic outgassing and LIBS

As discussed in the previous section, D release by ns-LIBS can come from two contributions: D content in the ablated surface layer and D that is thermally released from regions below the LIBS crater. In this section we analyse how much the contribution of thermal outgassing compared to ablation can be in conditions of the LIBS setup in PSI-2 [6].

As a first step we simulate the implantation phase using the 1D reaction-diffusion code CRDS [25]. For the sake of illustration, we take the model of retention and D transport from Hodille [10]. In that work three types of traps are assumed: two uniformly distributed intrinsic traps with de-trapping energies $E_1 = 0.87$ eV and $E_2 = 1.00$ eV, and trap concentrations $n_1 = 1 \times 10^{-3}$ at. fr. and $n_2 = 4 \times 10^{-4}$ at. fr., and one ion-induced near-surface trap type with de-trapping energy $E_3 = 1.50$ eV. Time evolution of ion-induced trap sites is described based on equation 11 and respective parameters from [10]. They have very high saturation concentration $n_{3a}^{max} = 10^{-1}$ at. fr. within the implantation zone of ~10 nm (supersaturation [26, 27]), and $n_{3b}^{max} = 10^{-2}$ at. fr. up to 1 µm depth. We use the most recent data for the lattice diffusion coefficient of D from [28] instead of commonly used Fraunfelder values [29]. This modification does not affect the assumptions and conclusions resulting from our simulations. Exposure conditions in the PSI-2 experiment are taken as reported in [6]: an exposure temperature of 650 K and an ion flux of $(2.7 - 5.2) \times 10^{21}$ $\frac{\text{ion}}{\text{m}^2\text{s}}$ (reflection neglected) depending on the radial position on the sample during 240 minutes of exposure. The flux variation comes from the hollow plasma profile of PSI-2 [6]. Simulated depth profiles of D at the end of exposure and retention as a function of exposure time are shown in figure 2 for the cases of the lowest and the highest experimental flux values. Considering retention in the first 100 nm (figure 2a), corresponding to the average LIBS crater depth in the PSI-2 experiment, at the end of exposure the first 10 nm contribute 63% to the retained D amount in the low flux case and 55% in the high flux case, dominated strongly by ion-induced traps. Figure 2b illustrates the reasoning presented in section 2: while total retention follows the $t^{0.5}$ dependence, retention in the first 100 nm grows faster due to trap creation at first and then tends to saturate.

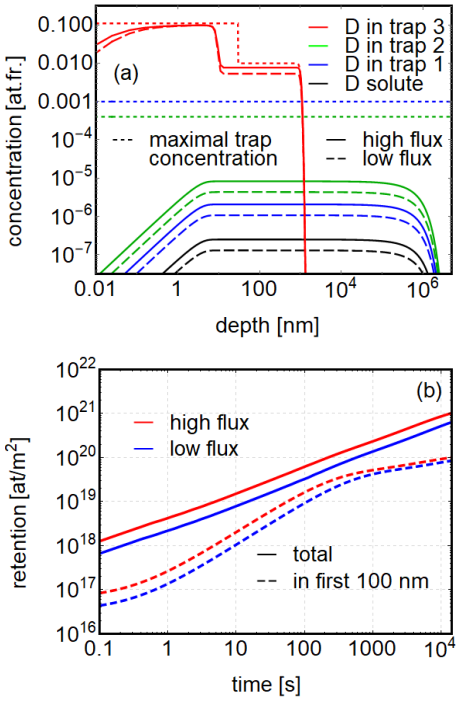

Figure 2. Simulated depth profiles of D at the end of exposure (a) and time evolution of total retention and retention in the first 100 nm (b) for the low flux (2.7×10^{21} $\frac{\text{ion}}{\text{m}^2\text{s}}$) and high flux ($5.2 \times 10^{21}$ $\frac{\text{ion}}{\text{m}^2\text{s}}$) cases.

As a next step we simulate D outgassing after plasma exposure. Figure 3a shows time traces of the passive outgassing flux for several assumptions regarding the sample temperature during outgassing. Based on experimental data [6] (figure 6 therein), cooling down of the sample can be fitted with a double exponential temperature decay with time constants of around 80 s and 400 s. However, as it can be seen from figure 3a, the outgassing flux under such conditions (labelled as "cooling") drops exponentially during the first 100 s, driven by de-trapping while the sample is still hot, and the decrease of retention does not reflect the expected power law dependence. Also, as it can be seen from figure 3b where evolution of retention in the first 100 nm is shown, fast sample cooling does not allow reproducing LIBS measurements from [6] (figure 7a therein). An extensive variation of input parameters of the diffusion-trapping model, including accounting for surface recombination with effective surface recombination coefficients typically used for W [30] did not lead to convincing results in favor of power law outgassing. Neither did it provide slow and moderate decay of the near-surface retention suggested by LIBS data. For this reason, outgassing at fixed temperatures between the exposure and room temperatures has been simulated to identify a reference case that could reproduce experimental trends. As can be seen from figure 3, the case of outgassing at 525 K follows closely the power law with $a \cong -0.7$, and at the same time shows a slow decay of the near-surface retention over 250 minutes comparable to LIBS data. Currently we have no other plausible solution. It is possible that the selected diffusion-trapping model validated on laboratory experiments with room temperature ion implantation [10] is not appropriate for high flux plasma conditions. This could be motivated by different dynamics of damage creation and trapping that eventually results in blistering at high implantation fluences, which is not taken into account by the model. In the following we shall nevertheless stick to this particular solution of outgassing at 525 K since it allows otherwise rather consistent illustration of LIBS temperature effects.

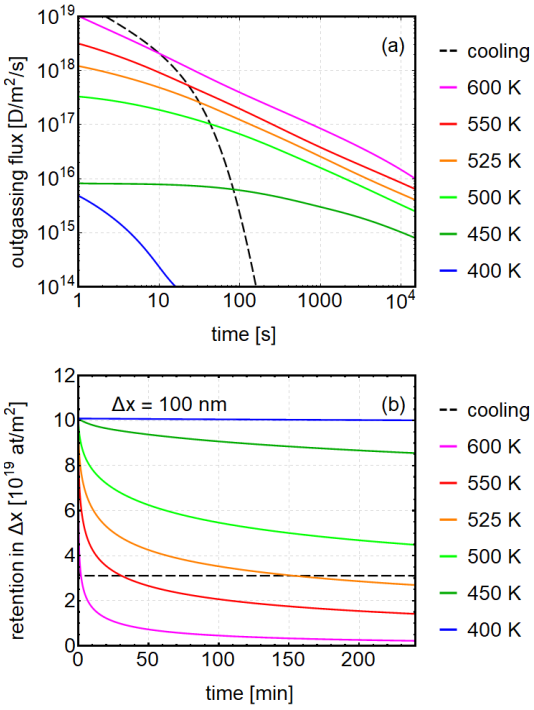

Figure 3. Simulated outgassing flux (a) and retention in the first 100 nm (b) during passive outgassing at different temperatures after the high flux (5.2×10^{21} $\frac{\text{ion}}{\text{m}^2\text{s}}$) exposure. The dashed lines correspond to the case of a gradual temperature variation during outgassing as a double exponential decay according to experimental data.

Simulations of material heating by laser are in general very complex [9, 31-35]. Since we are interested in thermal effects only beyond the ablated surface layer, we make a very rough estimate of temperature evolution by assuming that the material surface at the bottom of the crater during laser heating has a temperature either equal to the melting temperature of W, $T_m = 3695$ K, or to the boiling temperature, which we take equal to $T_b = 6000$ K [36]. In such a way we remove the heating source term and simulate heat propagation underneath the ablated crater during the laser pulse. In the after-pulse phase, we impose zero flux boundary condition at the surface and $T = 525$ K at the back of the sample (sample thickness 5 mm), consistent with the previous assumption on outgassing temperature. To simplify the calculation even further, we neglect the discontinuity of material thermal properties at $T = T_m$ [36] and estimate the

maximal possible heat penetration by using the highest value of the heat diffusivity in the temperature range from 300 K to 6000 K, which according to recommended data from [36] corresponds to $T = 300$ K and is equal to $\alpha = 7.12 \times 10^{-5}$ m^2/s. The resulting temperature evolution is shown in figure 4 for both temperature assumptions during the laser pulse.

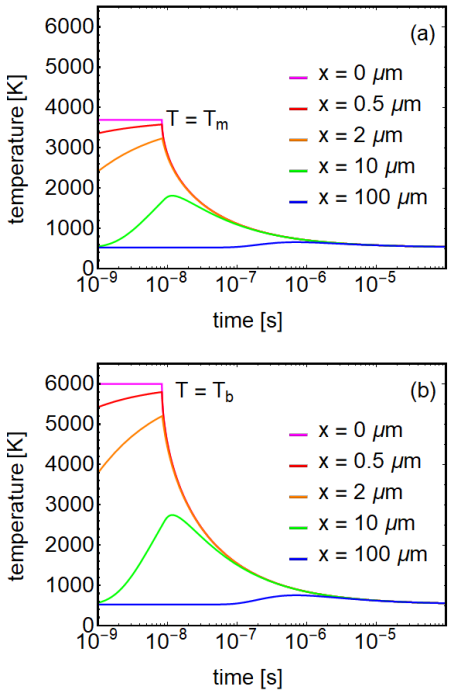

Figure 4. Simulated temperature evolution below a LIBS crater during and after a 8.3 ns laser pulse under the assumption of temperature equal to melting (a) or boiling (b) temperature of W at the bottom of the crater ($x = 0$).

Using these depth and time resolved temperature profiles during and after the laser pulse, we perform reaction-diffusion simulations with initial conditions corresponding to given points in time during the passive outgassing process. We assume that a layer of 100 nm is ablated by the laser and thus the temperature profile is applied to $x > 100$ nm. All depth profiles of D and trap concentrations are correspondingly shifted by 100 nm so that the first 100 nm corresponding to the ablated layer are removed. Figure 5 shows the respective amounts of thermally released D from a 100 nm thick layer below the LIBS crater for laser pulses at different times after the low flux exposure, given as absolute values (areal density), as fraction of available content in the respective layer, and as fraction of content within the LIBS crater (100 nm that have been removed by ablation). As follows from the data, thermal outgassing induced by LIBS contributes ~25% to the amount of D released by ablation in the first LIBS pulse performed right after plasma exposure and this fraction only increases for later pulses. This can be understood from Figure 6 that shows D depth profiles within the LIBS crater and below the crater before and after applying the laser (all trap contributions summed up) at $t = 0$ min and $t = 130$ min after the exposure: dynamic outgassing leads to a much stronger reduction of the concentration within the first 100 nm as compared to deeper regions.

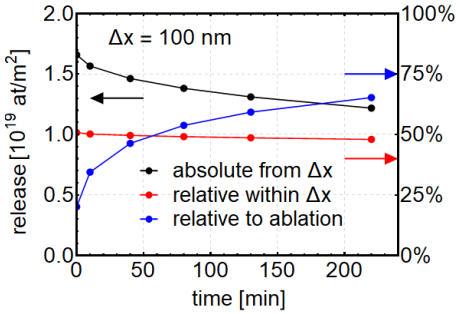

Figure 5. Simulated amounts of D thermally released from a layer of 100 nm thickness below the LIBS crater during and after laser pulses performed at different times after the low flux (2.7× 10^{21} $\frac{\text{ion}}{\text{m}^2\text{s}}$) exposure with $T = T_b$ at the bottom of the LIBS crater during the laser pulse.

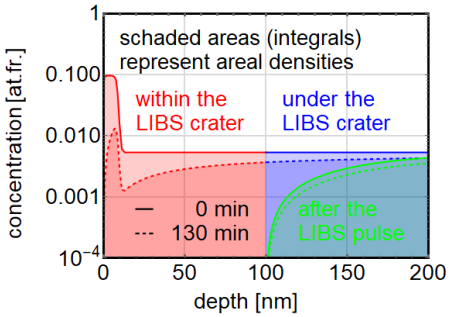

Figure 6. Simulated depth profiles of total D content within and below the LIBS crater before and after applying the laser at $t =$ 0 min and $t = 130$ min after the low flux (2.7× 10^{21} $\frac{\text{ion}}{\text{m}^2\text{s}}$) exposure with $T = T_b$ at the bottom of the LIBS crater during the laser pulse.

Finally, we perform simulations of multiple subsequent LIBS pulses with pulse repetition rate of 1 Hz at one location. For that we repeat the procedure of shifting the depth profiles by 100 nm after each pulse corresponding to ablation, and simulate additional thermal release from the remaining material. Figure 7 summarizes the reservoir for ablation by each LIBS pulse at $t = 0$ min after exposure, which can be compared to figure 2 in [6]. Very similar to the experimental data, the first LIBS pulse has access to a significantly larger D reservoir than subsequent pulses. In the simulated cases this is explained by two factors. Primarily, the first pulse removes the supersaturated 10 nm of the surface with the highest ion-induced trap concentration constituting over 50% of retention within the LIBS information depth (figure 5). Secondly, heating by laser results in thermal outgassing of up to 50% of the content within 100 nm below the LIBS crater (figure 5), thus reducing the content available for the subsequent LIBS pulse (figure 6). Consequently, these two factors lead to a reduction in the reservoir for ablation in the second pulse by about a factor of 4 compared to the first pulse. After 10 pulses the entire 1 µm layer with ion-induced traps is removed and only intrinsic traps with much lower trap concentrations and occupancies remain available, which significantly reduces the reservoir for subsequent pulses.

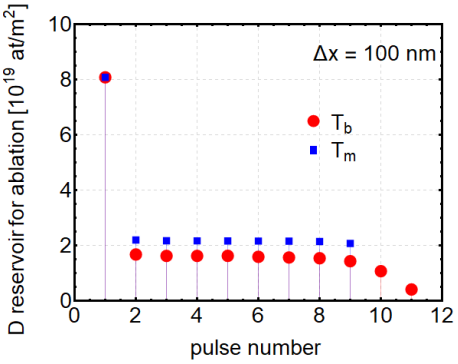

Figure 7. D reservoir available for ablation, calculated as the areal density of D within the surface layer of 100 nm thickness corresponding to the LIBS crater depth before each of repetitive (1 Hz) laser pulses at a single spot at $t = 0$ min after the low flux (2.7×10^{21} $\frac{\text{ion}}{\text{m}^2\text{s}}$) plasma exposure for two cases of temperature at the bottom of the LIBS crater during the laser pulse.

4. Summary

In this contribution we described and demonstrated with help of reaction-diffusion simulations the main concepts regarding short-term and long-term retention and related outgassing processes. Passive outgassing following plasma exposure was contrasted with temperature assisted outgassing, in particular with laser assisted outgassing in LIBS measurements. It was demonstrated that passive outgassing measured with the help of mass spectrometry on a global scale cannot be unambiguously inferred from a series of localized LIBS measurements, in particular because of intrinsically limited information depth accessible by LIBS. It was shown that thermal effects cannot be in general neglected in the case of ns-LIBS. In particular, in the simulated cases considered in this paper, which by design and parameter adjustement align well with LIBS experimental data from PSI-2 [6], thermal outgassing removes about 50% of D from a 100 nm thick W layer below the LIBS crater, contributing at least 25% to the amount of D released by ablation itself. Taking into account the conditions for heat propagation imposed in the model applied here, this result should be viewed as a rather extreme case. However, the contribution of thermal outgassing can potentially become even dominant if the technique is applied to deposited layers with their often porous structure and variable elemental composition, due to limited heat dissipation to the bulk of the underlying substrate material. Thus, such temperature effects have to be kept in mind for quantitative data analysis. Shorter laser pulses (fs- and ps-LIBS) can be recommended to reduce the respective uncertainty. Despite this word of caution, LIBS measurements represent a unique and powerful tool for local and in-situ analysis of retention evolution in fusion devices. In particular, measurements during exposure to plasma can provide valuable information about development of near-surface radiation damage, formation of supersaturated layers, co-deposition and modifications of surface morphology such as cracks or blisters that affect local retention.

Acknowledgements

This work has been carried out within the framework of the EUROfusion Consortium under work package PFC and has received funding from the Euratom research and training programme 2019–2020 under grant agreement No 633053. The views and opinions expressed herein do not necessarily reflect those of the European Commission.

References

[1] K. A. Moshkunov *et al* 2010 *Journal of Nuclear Materials* **404** 174 https://doi.org/10.1016/j.jnucmat.2010.07.011

[2] A. Drenik *et al* 2015 *Journal of Nuclear Materials* **463** 684 https://doi.org/10.1016/j.jnucmat.2014.12.084

[3] S. Musazzi and U. Perini (eds.), *Laser-Induced Breakdown Spectroscopy*, Springer Series in Optical Sciences **182** © Springer-Verlag Berlin Heidelberg 2014 https://doi.org/10.1007/978-3-642-45085-3

[4] A. Kreter *et al* 2015 *Fusion Science and Technology* **68** 8 https://doi.org/10.13182/FST14-906

[5] X. Jiang *et al* 2019 *Fusion Engineering and Design* **146** 96 https://doi.org/10.1016/j.fusengdes.2018.11.044

[6] X. Jiang *et al* 2021 *Nuclear Fusion* **61** 096006 https://doi.org/10.1088/1741-4326/ac112e

[7] M. Zlobinski *et al* 2020 *Physica Scripra* **T171** 014075 https://doi.org/10.1088/1402-4896/ab5ea1

[8] K. C. Phillips *et al* 2015 *Advances in Optics and Photonics* **7** 684 http://dx.doi.org/10.1364/AOP.7.000684

[9] Y. Jian-Jun *et al* 2007 *Chinese Physics* **16** 2003 https://doi.org/10.1088/1009-1963/16/7/033

[10] E. A. Hodille *et al* 2015 *Journal of Nuclear Materials* **467** 424 https://doi.org/10.1016/j.jnucmat.2015.06.041

[11] R. P. Doerner *et al* 2016 *Nuclear Materials and Energy* **9** 89 http://dx.doi.org/10.1016/j.nme.2016.04.008

[12] K. Schmid 2016 *Phisica Scripta* **T167** 014025 http://dx.doi.org/10.1088/0031-8949/T167/1/014025

[13] V. Philipps and J. Ehrenberg 1993 *Journal of Vacuum Science & Technology A* **11** 437 https://doi.org/10.1116/1.578750

[14] B. Pégourié *et al* 2011 *Journal of Nuclear Materials* **415** S809 http://dx.doi.org/10.1016/j.jnucmat.2010.10.071

[15] S. Panayotis *et al* 2013 *Journal of Nuclear Materials* **438** S1059 http://dx.doi.org/10.1016/j.jnucmat.2013.01.232

[16] V. Philipps *et al* 2013 *Journal of Nuclear Materials* **438** S1067 http://dx.doi.org/10.1016/j.jnucmat.2013.01.234

[17] S. Brezinsek *et al* 2013 *Nuclear Fusion* **53** 083023 https://doi.org/10.1088/0029-5515/53/8/083023

[18] S. Möller *et al* 2017 *Nuclear Fusion* **57** 016020 https://doi.org/10.1088/0029-5515/57/1/016020

[19] C. Grisolia, L. Horton, and J. Ehrenberg 1995 Journal of Nuclear Materials **220-222** 516 https://doi.org/10.1016/0022-3115(94)00514-1

[20] P. Andrew and M. Pick 1995 *Journal of Nuclear Materials* **220-222** 601 https://doi.org/10.1016/0022-3115(94)00548-6

[21] J. Guterl, R. D. Smirnov and S. I. Krasheninnikov 2014 *Contributions to Plasma Physics* **54** 415 https://doi.org/10.1002/ctpp.201410034

[22] S. I. Krasheninnikov and E. D. Marenkov 2014 *Physics Letters A* **378** 1526 https://doi.org/10.1016/j.physleta.2014.04.002

[23] S. I. Krasheninnikov *et al* 2014 *Physica Scripta* **T159** 014060 https://doi.org/10.1088/0031-8949/2014/T159/014060

[24] R. D. Smirnov *et al* 2014 *Contributions to Plasma Physics* **54** 610 https://doi.org/10.1002/ctpp.201410033

[25] D. Matveev *et al* 2018 *Nuclear Instruments and Methods in Physics Research B* **430** 23 https://doi.org/10.1016/j.nimb.2018.05.037

[26] L. Gao *et al* 2017 *Nuclear Fusion* **57** 016026 https://doi.org/10.1088/0029-5515/57/1/016026

[27] L. Gao *et al* 2020 *Acta Materialia* **201** 55 https://doi.org/10.1016/j.actamat.2020.09.065

[28] G. Holzner *et al* 2020 *Physica Scripta* **2020** 014034 https://doi.org/10.1088/1402-4896/ab4b42

[29] R. Frauenfelder 1969 *Journal of Vacuum Science and Technology* **6** 388 https://doi.org/10.1116/1.1492699

[30] O. V. Ogorodnikova 2019 *Journal of Nuclear Materials* **522** 74 https://doi.org/10.1016/j.jnucmat.2019.05.017

[31] P. Lorazo, L. J. Lewis and M. Meunier 2006 *Physical Review* B **73** 134108 http://dx.doi.org/10.1103/PhysRevB.73.134108

[32] B. N. Chichkov *et al* 1996 *Applied Physics A* **63** 109 https://doi.org/10.1007/BF01567637

[33] Y. Zhang *et al* 2017 *AIP Advances* **7** 075010 https://doi.org/10.1063/1.4995972

[34] A. H. A. Lutey 2013 *Journal of Applied Physics* **114** 083108 https://doi.org/10.1063/1.4818513

[35] A. V. Gusarov 2005 *Journal of Applied Physics* **97** 014307 https://doi.org/10.1063/1.1827321

[36] P. Tolias *et al* 2017 *Nuclear Materials and Energy* **13** 42 http://dx.doi.org/10.1016/j.nme.2017.08.002